

Belleri, A., Torquati, M., Marini, A., Riva, P.
Horizontal cladding panels: in-plane seismic performance in precast concrete buildings
(2016) Bulletin of Earthquake Engineering, 14 (4), pp. 1103-1129
DOI: 10.1007/s10518-015-9861-8
<http://link.springer.com/article/10.1007%2Fs10518-015-9861-8>

Horizontal cladding panels: in-plane seismic performance in precast concrete buildings

Andrea Belleri (*), Mauro Torquati, Alessandra Marini, Paolo Riva

Department of Engineering and Applied Sciences, University of Bergamo,
Viale Marconi 5, 24044, Dalmine – Italy

(*) corresponding author:

email: andrea.belleri@unibg.it; Tel. 0039 035 2052 007; Fax. 0039 035 2052 310;

Abstract

The paper investigates the in-plane performance of horizontal precast reinforced concrete (RC) cladding panels, typically adopted in one-storey precast industrial and commercial buildings.

Starting from in-field observations of cladding panels failures in recent earthquakes, the seismic performance of typical connections is evaluated by means of experimental tests on full-scale panels under quasi-static cyclic loading. The failure mechanisms highlight the vulnerability of such connections to relative displacements and, therefore, the need to accurately evaluate the connections displacement demand and capacity.

An analytical model is developed to describe the force-displacement relationship of the considered connections and compared to the experimental results. In order to determine the seismic vulnerability of such connections and provide design recommendations, linear and nonlinear analyses are conducted taking as reference a precast concrete structure resembling an industrial precast building. The results of the analyses show the importance of a correct estimation of the column's lateral stiffness in the design process and how an improper erection procedure leads to a premature failure of such connections.

Keywords: Precast concrete structures; Connections; Cladding panels; Seismic vulnerability.

1. Introduction

In industrial and commercial precast reinforced concrete (RC) buildings, cladding is typically provided by external heavy precast RC panels. The panels could be placed vertically, spanning from the ground to the roof without intermediate supports, or horizontally, supported by adjacent columns. Precast RC cladding are typically selected due to the fast erection time, the ability to cover long spans, the durability, fire safety and insulation properties (as in insulated sandwich panels) among others. In the case of horizontal cladding, more panels are positioned one over the other to cover the full building height.

According to Arnold (1989), the interaction between cladding and structural systems could be distinguished in: *completely separated cladding*, not interfering with the lateral stiffness and resistance; *accidentally participating cladding*, typically when the separation distance to the structural system is small compared to the seismic demand; *controlled participating cladding*, in which cladding contributes to the stiffening and dampening of the structure (Pinelli et al. 1995, 1996; NIST GCR 98-758; Ferrara et al. 2011); *fully participating cladding*, when cladding is fully integrated in the lateral force resisting system (Biondini et al. 2013; Magliulo et al. 2014a).

The most common connecting strategy adopted in high seismicity regions (NIST GCR 95-681) is to provide connections allowing relative movements between the cladding and the main structure, therefore aiming at *completely separated cladding* according to the aforementioned classification. In the United States of America bearing connections are placed at the bottom and rod connections at the top, the rods must be flexible enough to sustain the predicted range of movements and the bottom bearing connections should not be too rigid so as to avoid excessive stress concentration at the panel level. Such connections are typically referred to as “tie-back” connections. In New Zealand, the cladding lateral movements are accommodated by a sway mechanism in which sliding connections are provided by cleats bolted through slotted holes; however the sliding ability could be jeopardized by construction misalignment, flexure due to out-of-plane loads or bolts over-tightening. In Japan

(Wang 1987) vertical slotted connections are provided in order to achieve a rocking mechanism which better accommodates lateral drifts compared to rod connections, however requiring tightened tolerances and higher construction ability while suffering the same drawbacks of sliding connections. Considering specifically precast concrete industrial and commercial buildings, it is observed that these structures are generally more flexible compared to traditional RC frames due to the typical large inter-storey height and to the lateral force resisting system, which is usually composed of columns fixed at the base to isolated footings by means of mechanical splices (Metelli et al. 2011, Haber et al. 2014), grouted sleeves (Belleri and Riva 2012) or socket solutions (Osanai et al. 1996), and hinged at the top to pre-stressed RC beams. The lateral displacement demand is accommodated at the cladding panel level by relative displacements and rotations of the connections, owing to the higher stiffness of the RC panels compared to the connecting elements. Therefore, connections between precast secondary elements, as cladding panels, and the primary structure should be ductile enough to accommodate such displacements (Belleri et al. 2014a).

In the past Italian construction practice, precast cladding connections were mainly designed to allow for construction tolerance and to avoid out-of-plane overturning due to seismic loads. Although a limited amount of relative in-plane displacements is available also for such connections, the lack of specific detailing could lead to unintended participation of cladding panels during a seismic event and consequent failure of the connections, not designed to undergo the lateral displacements and rotations imposed by the earthquake, as highlighted by past seismic events (Toniolo and Colombo 2012; Liberatore et al. 2013; Belleri et al. 2014b; Magliulo et al. 2014b; Brunesi et al. 2015; Belleri et al. 2015), where several horizontal cladding panels fell down (**Fig. 1**).

In the case of an earthquake, cladding panels could be damaged if not properly detailed, causing a hazard to people outside the building and during evacuation procedures. Given the importance of such issues, experimental studies on cladding panel connections typically used in industrial buildings in Europe have been investigated (Colombo et al. 2014) and full-scale pseudo-dynamic tests have been carried out on specimens resembling single-storey buildings. Fischinger et al. (2014) and

Isakovic et al. (2014) report the performance of sliding connections, consisting of two anchor channels linked by a hammer-head strap. Uniaxial shear tests were mainly conducted under monotonic and cyclic loads. The type of failure recorded was dependent on the type of anchor channels: failure of the channel in cold formed channels and failure of the strap in hot rolled channels. The present paper considers typical horizontal cladding panel connections employed in industrial and commercial precast buildings in Italy, different from those presented in Fischinger et al. (2014) and Isakovic et al. (2014). Starting from full-scale tests of horizontal panel-to-columns subassemblies under quasi-static cyclic loading, the failure mechanisms are highlighted and an analytical model is developed to describe the force-displacement behaviour of such connections. Taking as reference a precast concrete industrial building, linear and nonlinear analyses are conducted to determine the seismic vulnerability of the investigated connections and to provide design recommendations.

2. Cladding panel full scale experimental campaign

2.1 Test setup and tested connections

Four full-scale cladding panel-to-column subassemblies (PCS) were tested under quasi-static reversed cyclic loading. Each subassembly (**Fig. 2**) is composed of two RC columns (0.5x0.5x3.0m) and one RC precast cladding panel (0.2x2.4x8.0m). The specimen layout and the element constraints are conceived to impose an assigned drift to the columns, which in turn enforces a defined deformation to the panel connections: a cylindrical hinge is provided at the base of the columns by means of a pin connection, while the column tips are mutually connected by a steel beam with pin connections at its ends. No axial load other than self-weight is acting on the columns. A cyclic horizontal displacement (**Fig. 2**) with increasing amplitude is imposed to the columns by an electromechanical screw jack. The horizontal load and column tip displacement are recorded by a load cell and by a displacement transducer respectively, while relative displacements between the panel connections and the columns are recorded by displacement transducers next to each connection.

The investigated connections, typical of existing horizontal precast claddings in Italy, are composed of bearing elements at the bottom and retaining elements at the top (**Fig. 3**). All the tested connections are proprietary devices of different Italian manufacturers and were provided according to their construction and design practice; in particular, each connection was selected by the manufacturer to cover construction tolerances and to sustain the gravity loads and out-of-plane seismic loads according to the tested cladding panel's geometry and to the design case study reported in the paper. Two bottom bearing connections were tested: the first connection (BC1 – **Fig. 3a**) is made of a rectangular steel element placed into a steel pocket inside the column during erection; the second connection (BC2 – **Fig. 3b**) is made of a steel plate rotating around a pivot point. The rotating plate is kept in the closed position, inside the column pocket, during transport and released during erection. In both bottom connection types, the horizontal seismic in plane loads are transferred by friction. The top retaining connection is characterized by three elements: a vertical anchor channel embedded in the column allowing for vertical tolerances; a slotted steel profile anchored into the panel for horizontal tolerances; a connecting flat head bolt with washers and nuts. Two types of top connections (TC1 and TC2 – **Fig. 3c 3d**), both characterized by 9 cm slotted holes, were tested.

The tested panel-to-column subassemblies (PCS) differ from each other by the connections. PCS A and PCS B present BC1 as a bottom connection and TC1 as a top connection. The top connection (**Fig. 4a**) is characterized by M16 class 5.6 bolts (BSI 2005) and cold formed anchor channels grade S250GD with 2.5 mm thickness. PCS A was intended to simulate a real construction scenario: top connection bolts tightened with unknown torque and horizontal misalignment (2 cm) to simulate construction tolerance. PCS B was intended to simulate a test under ideal conditions, with improvements regarding the top connection (**Fig. 4b**): a PTFE (polytetrafluoroethylene) film was added to the sliding surfaces to reduce friction; double nuts were placed to avoid tightening; the washer's diameter and thickness were increased.

PCS C and PCS D present BC2 as a bottom connection and TC2 as a top connection. The top connection is characterized by M14 class 5.6 bolts and cold formed anchor channels grade S350GD

with 2.5 mm thickness. PCS C adopts smaller diameter washers in the top connections (**Fig. 4c**) and a controlled tightening of the connecting bolts, in accordance to the manufacturer specifications. In PCS D a short steel tube was placed inside the slotted connection depth to allow sliding, meanwhile avoiding the effects of uncontrolled tightening of the connecting bolts (**Fig. 4d**).

2.2 Test results

The experimental results in terms of horizontal lateral load versus panel top displacement are presented in **Fig. 5**: the lateral load is representative of each top and bottom panel connection subassembly (PCS). The horizontal load arising due to second order P-Delta effects is negligible (1.7kN at a drift value of 4.2%) because no axial load other than self-weight is acting on the columns. Considering PCS A, it is observed that the uncontrolled tightening of the top connection bolts leads to unintended subassembly performance with no allowance for sliding. The assembly failed at the top connection due to plastic failure of the anchor channel (**Fig. 6a**) at a drift value of 1.04%, just above the serviceability limit state drift of 1.00%, typically adopted for the considered panels (EN 1998–1: 2004). In a real case scenario, this failure mechanism leads to a possible out-of-plane overturning of the panel, being the retaining ability of the top connection lost.

PCS B behaved as expected with low-friction sliding up to 1.00% drift due to the presence of the PTFE film applied to the sliding surfaces. The hysteretic behaviour changed once the washer reached the inner side of the slotted connection's pocket. At that point, the PCS stiffness is directly associated to the lateral stiffness of the bolt. The experimental test was stopped after concrete spalling of the panel top edge (**Fig. 6b**), corresponding to 2.1% drift, at a lateral force value close to the anchor channel failure recorded during PCS A testing.

PCS C and PCS D exhibited very similar results. The increased lateral displacement capacity is associated to the higher horizontal clear space of the top connection pocket and to the activation of sliding at the bottom connection, being the latter associated to the higher capacity of TC2 with respect to TC1. Once the free sliding capacity of the top connection is reached, the lateral force increases

until overcoming the friction of the bottom connection, approximately at 2% drift. When the bottom connection reaches its free sliding capacity, approximately at 3.5% drift, there is a gain of lateral stiffness and an increase of the lateral load, until shear failure of the top connection (**Fig. 6c**), at the bolt anchor head; when the nut touches the panel side (**Fig. 6c**), the top connection's load path changes. The connection failure happened at approximately 4.5% drift.

It is important to note that the top connection sliding ability is enhanced by a controlled tightening of the connecting bolt or by the use of a steel tube placed inside the slotted connection depth (PCS D). In addition, the use of the PTFE film in TC1 (PCS B) reduced by half the friction load of the top connection with respect to TC2 (PCS C and D); this reduction is thought as non-critical for the good performance of the top connection.

3. Connections analytical formulation

This section presents a simplified analytical formulation of the tested connections in order to define a hysteretic model suitable for numerical simulations and to provide a conservative estimation of the connection capacity. The top and bottom connections are treated separately.

Regarding the top connection, the load–displacement relationship is obtained considering the contribution of the anchor channel, the slotted connection and the bolt according to the static scheme of **Fig. 7a**. The influence of nuts and washers is taken into account by reducing the clear length L_b of the connecting bolt.

Spring S1 is considered as elasto-plastic with a yield moment ($M_{y,S1}$) corresponding to the flexural capacity of the slotted plate. The elastic stiffness is obtained treating the slotted plate as a fixed ends beam. In the case of a concentrated moment in the slotted plate centreline, the elastic rotational stiffness ($k_{\theta,S1}$) is equal to $16 EI_{sl}/L_{sl}$, where EI_{sl} and L_{sl} are the flexural stiffness and length of the slotted plate, respectively.

Spring S2 is considered as elasto-plastic with a yield moment value corresponding to the capacity of the channel lip when subjected to the distributed load p , F being its resultant, transferred by the headed bolt during the rotation around point A (**Fig. 8a**).

The maximum force F_{max} is obtained according to the yield line theory with the distribution shown in **Fig. 8c**, assuming α equal to 45° :

$$F_{max} = f_u \cdot s^2 \cdot \left(4 + \frac{i}{2t} \right), \quad (1)$$

where i , s and t are shown in **Fig 8** and f_u is the yield stress of the anchor channel steel. The channel capacity is calculated supposing that the contact between the bolt and the channel is provided along the whole length of the channel lips. This assumption is considered realistic in the evaluation of the channel yield capacity. At the ultimate limit state, the contact between the channel and the anchor bolt is limited to a smaller area, due to large deformations and rotations of the screw and the channel. This leads to an increase of the lever arm between the contact-force resultant and the pivot point, which, in turns, leads to an increase of the bending moment capacity. Such behaviour is not included in the previous equation, which, therefore, provides a conservative estimate of the connection capacity. The derivation of Eqn. 1 is reported in Appendix A.1.

To allow for a simplified estimate of the channel lip displacement (Δ), an equivalent cantilever beam is introduced with thickness s , length t , and depth b_{eq} . The equivalent depth b_{eq} is derived (Eqn. 2) by equating the displacement of such beam to the displacement of the anchor channel lip, treated as a cantilever plate (**Fig. 9**). The displacement of the anchor channel lip is obtained from 3D elastic finite element analyses (Abaqus 2011).

$$\begin{cases} (b_{eq} - i)/(2t) = 1 & \text{for } 3.75 < t/s \leq 10 \\ (b_{eq} - i)/(2t) = 0.09 \cdot t/s + 0.66 & \text{for } 1.875 \leq t/s \leq 3.75 \end{cases} \quad (2)$$

The lateral displacement of the equivalent beam, including shear deformations, is:

$$\Delta_{eq} = \frac{3}{10} \frac{F \cdot t}{b_{eq} \cdot s} \left(\frac{5 \cdot t^2}{E \cdot s^2} + \frac{2}{G} \right) \quad (3)$$

where G is the steel shear modulus. The derivation of Eqn. 3 is reported in Appendix A.2.

To account for the flexibility of the anchor channel's side, the displacement associated to the rotation around point B (**Fig. 8**) is included in the previous expression; this is accomplished by considering the anchor channel's side as a fixed end cantilever subjected at its tip to the bending moment related to F (derivation in Appendix A.3):

$$\Delta_{tot} = \Delta_{eq} + \frac{3}{2} \frac{F \cdot h \cdot t^2}{E \cdot b_{eq} \cdot s^3} \quad (4)$$

where h is the anchor channel depth (**Fig. 8a**). The yield displacement, according to the proposed elasto-plastic formulation, is obtained by substituting the maximum force F_{max} into the previous equation. The maximum displacement ($\Delta_{u,tot}$) recorded from experimental tests on the considered anchor channels is approximately equal to $0.4 t$. Based on these results, the moment-rotation relationship of spring S2 is obtained considering $M_{y,S2} = M_{u,S2} = F_{max} d$, $\theta_{y,S2} = \Delta_{tot,y}/e$ and $\theta_{u,S2} = \Delta_{tot,u}/e$. The elastic rotational stiffness ($k_{\theta,S2}$) is equal to $M_{y,S2}/\theta_{y,S2}$.

According to the static scheme depicted in **Fig. 7a**, the lateral stiffness of the top connection (k_{TC}) is equal to:

$$k_{TC} = \frac{12 \cdot EI_b}{L_b^2} \frac{EI_b \cdot (k_{\theta,S1} + k_{\theta,S2}) + k_{\theta,S1} \cdot k_{\theta,S2} \cdot L_b}{(12 \cdot E^2 I_b^2 + 4 \cdot EI_b \cdot (k_{\theta,S1} + k_{\theta,S2}) \cdot L_b + k_{\theta,S1} \cdot k_{\theta,S2} \cdot L_b^2)} \quad (5)$$

The elastic rotations (θ_{S1} , θ_{S2}) at the bolt ends, necessary to evaluate the bending moments of springs S1 and S2 in the elastic range, depend on the lateral load (V) acting on the connection:

$$\theta_{S1} = \frac{VL_b}{2} \frac{2EI_b + k_{\theta,S2}L_b}{EI_b(k_{\theta,S1} + k_{\theta,S2}) + k_{\theta,S1}k_{\theta,S2}L_b}; \quad \theta_{S2} = \frac{VL_b}{2} \frac{2EI_b + k_{\theta,S1}L_b}{EI_b(k_{\theta,S1} + k_{\theta,S2}) + k_{\theta,S1}k_{\theta,S2}L_b} \quad (6, 7)$$

Being the springs S1 and S2 in series with the bolt, the first plastic hinge is associated to the flexural capacity of the weakest component, corresponding to the anchor channel for TC1 and to the bolt for

TC2. Once the first plastic hinge occurs, provided there is enough ductility, the connection is still able to carry additional lateral loads until the onset of a plastic hinge at the other end. After the development of both plastic hinges, the connection rotates (**Fig. 7b**) and the panel moves towards the column until it reaches the contact. At this stage, tensile stresses arise in the bolt, due to the rope effect, until the failure of a component. In the case of TC1, the connection failure occurs when the displacement capacity of the anchor channel lip is overcome, following the development of the first plastic hinge. In the case of TC2, the connection failure is associated to the achievement of the shear capacity in the bolt after the development of plastic hinges at the bolt ends.

The inclusion of sliding in the above formulation is straightforward. Starting from the force-displacement curve in the no-sliding case, once the friction force $F_{frict,TC}$ is achieved, the connection slides laterally at a constant force; the sliding continues until contact occurs between the washer and the connection pocket side or between the bolt and the slot's end, whichever happens first. After contact, the force-displacement curve resumes from the point where it was interrupted.

Regarding the bottom connection, the lateral force-displacement relationship is directly evaluated considering the bolt flexibility for BC1 and the flexural stiffness of the tapered steel plate for BC2. As for the top connection, once the friction force $F_{frict,BC}$ is achieved, the bottom connection starts sliding. $F_{frict,BC}$ is a function of the bolt-panel friction coefficient (μ_{BC}) and the vertical load (N_{BC}), the latter being typically equal to half of the panel's weight. The coefficient of friction could achieve high values in the case of roughened surfaces.

The proposed analytical formulation is applied to the tested specimens. The top connections of PCS A are modelled directly with a spring element with a Clough hysteretic model, being the sliding activation load higher than the connection's capacity. All the other connections are modelled with overlapped non-linear springs (Appendix A.4): slip-trilinear springs account for the connection's behaviour after free sliding, and normal-bilinear springs account for friction. **Fig. 10** shows the scheme of the finite element model used in the simulation of the quasi-static experimental tests.

Fig. 11 shows the comparison between numerical and experimental results. An overall good matching

between the experimental results and the analytical formulation is observed, although the proposed formulation is unable to capture the larger energy dissipation capacity associated to PCS C and D.

4. Numerical simulations

To evaluate the seismic performance and design implications of the tested connections, a case study resembling a typical industrial precast building is considered. The structural layout is shown in **Fig. 12**. Cantilever columns (7.2 m tall) constitute the lateral force resisting system. The columns have a square cross-section (0.6x0.6 m) reinforced with 16 longitudinal 18 mm diameter bars, equally distributed along the edges. The resulting longitudinal reinforcement ratio is equal to 1.1%. The concrete cover is 40 mm. The columns support 9 cladding panels along the building longitudinal side. The considered cladding panels have the same geometry of the tested specimens (2.4x8.0x0.2 m). No mutual constraint between adjoining panels is considered. The roof's tributary mass acting on the corner and inner columns are equal to 33'000 kg and 66'000 kg respectively.

The seismic design complies with EN 1998–1: 2004 (BSI 2005) type 1 elastic spectrum, soil type A and a peak ground acceleration (PGA) of 0.35 g at the design basis earthquake (DBE) limit state. The adopted behaviour factor is 2. A column's bending stiffness equal to half of the gross section stiffness is used to account for concrete cracking (BSI 2005). For the serviceability limit state (SLS) earthquake, the elastic spectrum is obtained dividing by 2.5 the DBE elastic spectrum. The resulting inter-storey drift, defined as the ratio between lateral displacement and inter-storey height, is 0.4% and 1.0% for SLS and DBE respectively.

The low value of the adopted behaviour factor is a result of the design process, which is governed by the code limitation on second order effects. The obtained interstorey drift sensitivity coefficient (EN 1998–1: 4.4.2.2.2), corresponding to the ratio between second order and first order column moments, is less than 0.1. This allows overcoming the requirement (EN 1998–1: 5.4.1.2.2) on the cross-section dimensions of primary seismic columns, which should be larger than one tenth of the larger distance

between the point of contraflexure and the ends of the columns (7.2 m, based on the considered static scheme). Such a requirement is mandatory only if the interstorey drift sensitivity coefficient is greater than 0.1.

Higher values of the behaviour factor would reduce the seismic demand, as for instance the bending moment at the column base, but would lead to an interstorey drift sensitivity coefficient greater than 0.1, therefore to columns with a minimum cross-section side equal to 0.72 m, compared to 0.6 m provided herein. In addition, in the considered case study, the requirement for minimum longitudinal steel ratio (1%) leads to a bending moment capacity much higher than required; therefore the effective behaviour factor, corresponding to the ratio between the elastic demand and capacity, is lower than expected. Other authors (Fischinger et al. 2014) also addressed the higher relevance of drift and slenderness limitations requirements compared to the behaviour factor in these types of structures.

4.1 Fragility analysis

To highlight the seismic vulnerability of precast cladding in industrial buildings, a fragility analysis is carried out based on the tested connections. The lateral frame presented in **Fig. 12** is considered. Nonlinear time history analyses are conducted with the software MidasGEN (2012), modelling the panels as elastic beams connected to the columns by means of non-linear springs according to the scheme of **Fig. 10**. The panel mass is directly included in the model by assigning a mass density to the corresponding beam element. The columns are fixed at the base and modelled with nonlinear fiber elements; the concrete's 28-day cylindrical strength is equal to 40 MPa and the yield stress of the steel reinforcement is equal to 450 MPa. Three models are analysed, differing from each other by the panel-to-column subassembly considered (PCS A, PCS B and PCS C/D). **Fig. 13a** shows a scheme of the finite element model.

A set of thirty recorded earthquakes¹ were selected and scaled from the European strong motion database (Ambraseys et al., 2004) to match the DBE elastic spectrum (**Fig. 14**). The same strategy adopted by Kramar et al. (2010) is considered herein: a single set of accelerograms is used for all intensity levels, beside the fact that earthquake records should be reselected at each intensity in accordance to the change of hazard level (Baker and Cornell 2006). The PGA is selected as intensity measure (Kramar et al. 2010) and incremental dynamic analyses (Vamvatsikos and Cornell 2002) are conducted at approximately 0.05 g PGA-intervals. Two damage states are considered for each model: connection yielding (DS1-A) and failure (DS2-A) for the model implementing PCS A connections; end of free-sliding (DS1-B) and connection failure (DS2-B) for the model implementing PCS B connections; end of free-sliding (DS1-C/D) and connection failure (DS2-C/D) for the model implementing PCS C/D connections.

For each intensity level, the fragility curve is constructed evaluating the exceedance ratio of each damage state and considering a lognormal distribution. The parameters of the lognormal distribution (the mean and the standard deviation) are estimated by the least square method. **Fig. 15** shows the fragility curves associated to the 3rd row of cladding panels, in terms of cumulative probability of exceedance (P). The 3rd row is selected due to the higher relative displacements between top and bottom connections resulting from the lateral deflection of cantilever columns under seismic loads. The obtained fragility curves highlight the higher vulnerability of PCS A, i.e. not controlled connections, compared to PCS B: the expected failure of PCS A and PCS B are associated to a PGA equal to 0.18 g and 0.32 g, respectively. In addition, it is observed that yielding of PCS A, damage state DS1-A, occurs at low-intensity levels, sensibly reducing any eventual stiffening effect provided by the cladding panels. As expected, PCS C/D vulnerability is lower than PCS B: the expected failure

¹ Record codes of the considered earthquakes according to Ambraseys et al. 2004: 0034xa, 0050x, 0051xa, 0084ya, 0120ya, 0146ya, 0212ya, 0306ya, 0317xa, 0322ya, 0333ya, 0335ya, 0341ya, 0343ya, 0385ya, 0388ya, 0389xa, 0390xa, 0393ya, 0412ya, 0421xa, 0437ya, 0438xa, 0438ya, 0442xa, 0443xa, 0444ya, 0451xa, 0457ya, 0461ya

of PCS C/D is associated to a PGA equal to 0.45 g. It should be pointed out that the results are based on soil type A (BSI 2005). Different soil conditions would lead to different results.

4.2 Design implications

Eigenvalue, response spectrum, pushover and time history analyses are conducted to highlight the connection performance and to derive design implications. Two additional finite element models are considered. The first model (*PCS ideal*) is based on **Fig. 13a** and represents ideal conditions of the panel-to-column connections: the bottom connections are modelled as hinges and the top connections as rollers. The second model (*Point mass*) represents the typical configuration used in the design practice: each panel is modelled directly with point masses on the supporting columns at a height corresponding to the panel's centroid (**Fig. 13b**).

Eigenvalue and response spectrum analyses are conducted taking into account the equivalent stiffness of columns (Appendix A.5). **Table 1** shows the results of the eigenvalue analysis in terms of period (T_i) and mass participation factor (m_i) of the first three modes of vibration, showing an increase of stiffness in the fundamental mode and negligible differences of the mass participation factor when cladding panel connections are included.

Table 2 shows the results of the response spectrum analysis in terms of maximum column base shear, inter-storey drift and top row PCS rotation; the PCS rotation is defined as the ratio between the relative displacement of the top and bottom connections and the panel height. As expected, following the stiffness increase reported in **Table 1**, the models including the panel connections (PCS A/B and PCS C/D) present higher column base shear, smaller lateral displacements and smaller PCS rotations compared to the models with either no connections (*Point mass*) or ideal connections (*PCS ideal*).

The previous results are based on cladding panel connections acting as elastic springs, with stiffness equal to their initial stiffness. In accordance to this assumption, each connection should be designed to carry the seismic load demand resulting from the analysis. This would lead to a “*fully participating cladding*” behaviour, which is not the case of the considered connections.

Pushover and time history analyses are conducted to investigate the effectiveness of the stiffening effect and the connections performance once sliding occurs. The pushover analyses are carried out by means of a lateral force distribution according to the fundamental mode of vibration. The time history analyses are carried out by means of artificial spectrum-compatible records (SLS and DBE) generated with the SIMQKE-1 algorithm (Venmarcke and Gasparini, 1976).

Fig. 16 shows the pushover results in terms of total base shear versus roof displacement. In the case of PCS A, all the connections fail well before yielding of the columns, confirming how an improper erection procedure could lead to an anticipated connection failure and consequently possible panel out-of-plane overturning. Similar results are obtained for PCS B, in which the sliding ability of the top connection delayed its failure; both 3rd and 2nd row panels fail before yielding in the columns. In the case of PCS C/D the failure of the connection is beyond yielding of the columns, owing to the higher PCS rotation capacity. It is worth noting that sliding occurs at the beginning of the analysis in both PCS B and PCS C/D.

Table 3 contains the results of the nonlinear time history analyses. It is observed how the stiffening effect of the connections is relevant only in the SLS analyses. DBE analyses lead to similar results regardless of the considered model, owing to the sliding ability and limited capacity of the connections, which reduce the interaction between the cladding panels and the supporting structure. The PCS rotation demand is higher than the roof drift demand, resulting from the lateral deflection shape of cantilever columns.

It is observed that the roof drift demand is higher than computed during the design process (0.4% for SLS and 1.0% for DBE). This is related to the reduction of the column flexural stiffness to account for concrete cracking: during design the stiffness was reduced by half according to EN 1998-1: 2004 (BSI 2005) although the actual secant stiffness at yield, evaluated by means of a cross section moment curvature analysis, is 28% of the gross section stiffness (Appendix A.5). It is worth noting that the foundation flexibility could further increase the relative displacement demand of the panel connections.

Considering the *Point mass* model, the SLS results are conservative both in terms of PCS rotation and column base shear; the DBE results are slightly underestimated, with differences at most equal to 3.7%, 4.7%, and 6.5% for column base shear, inter-storey drift and PCS rotation respectively. Hence, this simplified model is suitable to determine the PCS rotation demand for the investigated connections, especially when sliding occurs (PCS B and PCS C/D).

Beside these results, it is worth comparing the response spectrum and time history output for the *Point mass* model. The comparison shows significant underestimation of the DBE response spectrum results. This is related to the difference between the nominal behaviour factor used in the design ($q=2$) and the effective behaviour factor ($q_{eff}=1.45$), obtained as the ratio between the column elastic demand (945 kNm) and flexural capacity (650 kNm). This difference arises from limiting the interstorey drift sensitivity coefficient below 0.1 (control of second order effects) and from providing minimum longitudinal steel ratio (1%), as mentioned before. A response spectrum analysis with the effective reduction factor leads to a column base shear, inter-storey drift and PCS rotation demand equal to 109.2 kN, 1.40% and 2.05% respectively, very close to the time history results. Therefore, the *Point mass* model is suitable to determine the PCS rotation demand if the effective behaviour factor is used in response spectrum analyses.

To avoid unintended connection failures and consequent panel overturning, it is recommended to design the top connections with enough sliding capacity to accommodate the PCS rotation demand associated to the DBE limit state. In such a case, the PCS rotation capacity is equal to the ratio between gap_{TC} and the distance between top and bottom connections. In addition, the failure of the top connection should follow the sliding load (due to friction) of the bottom connections to accommodate a higher PCS rotation demand, arising, for instance, from higher intensity seismic events or from connection misalignments. This detail allows the activation of sliding of the bottom connections leading to an increase of the PCS rotation capacity, which, in this case, is equal to the ratio between $(gap_{TC} + gap_{BC})$ and the distance between top and bottom connections.

Regarding the bottom connections, it is observed that each connection contributes to carrying the panel in-plane inertia load. However, it is suggested to conservatively design each bottom connection to sustain the whole panel inertia load, to account for the possible and worst case scenario in which only a single BC reaches contact to the panel side as a consequence of connection misalignments and tolerance issues. This situation leads to an increase of the connection lateral stiffness with a consequent redistribution of the panel inertia load among the connections.

Another important aspect is the implication of the cladding panels in the capacity design of columns. Taking as reference a single column, the ratio between the tributary mass of cladding panels and the roof tributary mass could be high (44% in the present case study), leading to a reduction of the column effective height and, therefore, to an increase of the column's shear demand.

Finally, it is worth noting that the post-earthquake inspections of existing cladding panel connections could be a difficult task, being the horizontal cladding connection zones typically hidden at the column-to-panel interface for fire safety and aesthetic reasons. Back-up connections could be installed on existing cladding panels to overcome this limitation and avoid panel overturning after the failure of top connections. **Fig. 17** shows possible back-up solutions to be installed at the top of the panels: on the left a steel bracket with a slotted hole; on the right a steel wire rope. Both solutions need to accommodate the PCS rotation demand and to sustain the out-of-plane loads. The evaluation of out-of-plane loads on top and bottom connections is the topic of an ongoing research.

5. Conclusions

The present paper investigated the seismic performance and design implications of precast horizontal panels typically adopted as cladding in precast reinforced concrete industrial and commercial buildings. An experimental campaign was conducted on four full-scale cladding panel-to-column subassemblies with typical connections adopted in Italy. The experimental results highlighted failure mechanisms associated to the top connections. In the case of uncontrolled anchor bolt tightening, the

sliding ability is inhibited and an anticipated connection failure is recorded. This leads to a possible panel out-of-plane overturning. The inclusion of a short steel tube placed inside the slotted connection depth is a simple detail able to avoid uncontrolled tightening of the connecting bolts during erection. A simplified analytical formulation was derived to define hysteretic models suitable for numerical simulations of the tested and similar connections. Sliding connections are modelled with overlapped nonlinear springs: slip-trilinear springs accounting for the free sliding ability; normal bilinear springs accounting for friction. The model was validated against the full-scale experimental results.

A case study resembling an industrial building was selected. Seismic analyses were conducted to highlight the performance of the considered connections and to provide design recommendations.

The main findings are summarized in the following.

- An accurate evaluation of the column secant stiffness at yield is necessary to guarantee a correct estimation of the rotation demand of the panel-to-column subassembly (PCS).
- The PCS rotation demand is higher than the roof drift demand due to the lateral deflection shape of cantilever columns.
- The considered connections are difficult to inspect after an earthquake, being the horizontal cladding connection zones typically hidden at the column-to-panel interface as a fire safety measure and for aesthetic reasons. Back-up connections could be installed on existing cladding panels to avoid panel overturning after the failure of top connections.
- It is recommended to design the top connections with sufficient sliding capacity as to accommodate the PCS rotation demand at the design basis earthquake (DBE).
- It is recommended to design the top connection with a failure load higher than the bottom connection friction load. This detail increases the PCS rotation capacity.
- Following the previous recommendations, the stiffness of the panel and the stiffness of the connections do not affect the structural response at the DBE. In fact the panels do not contribute to the stiffness of the structure due to the relatively small stiffness of their connections. Therefore

the evaluation of the PCS rotation demand can be determined by means of a *Point mass* finite element model: each panel is modelled directly with point masses on the supporting columns at a height corresponding to the panel centroid. Typical response spectrum analyses are suitable to determine the PCS rotation demand, providing that the effective behaviour factor is adopted.

- Each bottom connection should be designed to sustain the whole panel inertia load. This case represents the worst scenario: the contact between the bottom connection and the panel side is associated to an increase of the connection lateral stiffness with a consequent redistribution of the panel inertia load.

Horizontal heavy cladding influences the capacity design of columns: the column effective height reduces and the base shear demand increases. The effective height's reduction is associated to the distribution of the inertia loads on the panels, which, in the in-plane direction, are transferred to the columns by the panel's bearing connections.

The analysis of the in-plane behaviour of vertical cladding panels and the evaluation of the out-of-plane seismic loads on panel connections are the topics of ongoing research.

Acknowledgements

The authors wish to express their gratitude to Assobeton (Italy) for financing the experimental campaign. The opinions, findings, and conclusions expressed in the paper are those of the authors. The careful review and constructive suggestions by the anonymous reviewers are gratefully acknowledged.

LIST OF ACRONYMS

BCx bottom connection x

DBE design basis earthquake

DSx-y damage state x for PCS-y

PCS-x	panel to column subassembly x
PGA	peak ground acceleration
S1	spring representing the slotted plate flexural behaviour (TC)
S2	spring representing the anchor channel flexural behaviour (TC)
SLS	serviceability limit state
TCx	top connection x

LIST OF SYMBOLS

b_{eq}	depth of equivalent cantilever beam representing anchor channel lip
d	distance represented in Fig. 8a
e	distance represented in Fig. 8a
E	Young modulus of steel
EI_b	flexural stiffness of the TC bolt
EI_{sl}	flexural stiffness of the TC slotted plate
F	force resultant on channel lip due to distributed load p
$F_{frict,x}$	friction force of connection x
f_u	ultimate stress
gap_x	horizontal gap (Fig. 7) in the x connection (TC or BC)
gap_v	clear length between the panel and the column (Fig. 7)
G	steel shear modulus
h	anchor channel depth (Fig. 8)
i	anchor bolt head thickness (Fig. 8)
$k_{\theta,Sx}$	elastic stiffness of connection Sx
L_b	clear length of the TC connecting bolt
L_{sl}	length of the TC slotted plate

μ	coefficient of friction of bottom connection
m_i	mass participation factor of mode i^{th}
$M_{u,Sx}$	ultimate flexural capacity of connection Sx
μ_x	coefficient of friction of connection x
$M_{y,Sx}$	yield flexural capacity of connection Sx
N_{BC}	vertical load acting on bottom connection
P	cumulative probability of exceedance
p	distributed load on anchor channel lips
s	anchor channel thickness (Fig. 8)
t	anchor channel lip length (Fig. 8)
T_i	period of vibration of mode i^{th}
V	lateral load acting on the connection
Δ_{eq}	anchor channel lip displacement neglecting the contribution of anchor channel side rotation
Δ_{tot}	anchor channel lip displacement including the contribution of anchor channel side rotation
θ_{Sx}	rotation of spring Sx

APPENDIX A

A.1 Derivation of Equation 1

According to the yield line theory, adopting the yield line pattern shown in **Fig. 8c** and α equal to 45° , the work (W_{ext}) done by the external load (**Fig. 8b**) is:

$$W_{ext} = \int_0^t p \cdot \Delta(x) \cdot dx = \int_0^t p \cdot \theta \cdot x \cdot dx = p \cdot \theta \cdot \frac{t^2}{2} = F \cdot \theta \cdot \frac{t}{2} \quad (\text{A1.1})$$

where θ is the imposed rotation of the plate around yield line 2 (YL₂).

The internal work (W_{int}) is:

$$\begin{aligned}
W_{\text{int}} &= 2 \int_{YL_1} M_{pl} \cdot \theta \cdot dx + \int_{YL_2} M_{pl} \cdot \theta \cdot dx + 2 \int_{YL_3} M_{pl} \cdot \sqrt{2} \cdot \theta \cdot dx = \\
&= 2M_{pl} \cdot t \cdot \theta + M_{pl} \cdot (2t + i) \cdot \theta + 4M_{pl} \cdot t \cdot \theta = M_{pl} \cdot (8t + i) \cdot \theta
\end{aligned} \tag{A1.2}$$

Equating the external and internal work leads to:

$$\begin{aligned}
W_{\text{int}} = W_{\text{ext}} \quad \rightarrow \quad M_{pl} \cdot (8t + i) \cdot \theta &= F \cdot \theta \cdot \frac{t}{2} \\
F = M_{pl} (8t + i) \frac{2}{t} = \frac{f_u \cdot s^2}{4} (8t + i) \frac{2}{t} &= f_u \cdot s^2 \left(4 + \frac{i}{2t} \right)
\end{aligned} \tag{A1.3}$$

A.2 Derivation of Equation 3

The lateral deflection Δ of a cantilever beam with uniform cross section and length t under a uniform distributed load p is:

$$\Delta(x) = \Delta_{\text{flexure}}(x) + \Delta_{\text{shear}}(x) = \frac{p \cdot x^2}{24EJ} (x^2 + 6 \cdot t^2 - 4 \cdot t \cdot x) + \frac{p}{GA_s} \left(t \cdot x - \frac{x^2}{2} \right) \tag{A2.1}$$

By evaluating the previous equation for $x = t$ and by considering a rectangular cross section $b_{eq} \times s$ with a shear area $A_s = 5/6 A$, it yields:

$$\Delta(t) = 3 \cdot t^2 \frac{p \cdot t^2}{24EJ} + \frac{p}{GA_s} \frac{t^2}{2} = 3 \cdot t^2 \frac{F \cdot t}{24E \frac{b_{eq} s^3}{12}} + \frac{F}{G \frac{5}{6} b_{eq} s} \frac{t}{2} = \frac{3}{10} \frac{F \cdot t}{b_{eq} \cdot s} \left(\frac{5 \cdot t^2}{E \cdot s^2} + \frac{2}{G} \right) \tag{A2.2}$$

A.3 Derivation of Equation 4

Considering the vertical side of the channel (**Fig. 8**) as a cantilever with height equal to h and subjected to a tip moment equal to $F \cdot t/2$, the tip rotation is:

$$\theta_{\text{tip}} = (F \cdot t/2) \frac{h}{4EJ} \tag{A3.1}$$

This rotation leads to an additional channel lip deflection equal to:

$$\Delta_{rot} = \theta_{tip} \cdot t = F \cdot t^2 \frac{h}{8EJ} = F \cdot t^2 \frac{h}{8E \frac{b_{eq} s^3}{12}} = \frac{3}{2} \frac{F \cdot h \cdot t^2}{E \cdot b_{eq} \cdot s^3} \quad (A3.2)$$

Therefore the total displacement is:

$$\Delta_{tot} = \Delta_{eq} + \Delta_{rot} = \Delta_{eq} + \frac{3}{2} \frac{F \cdot h \cdot t^2}{E \cdot b_{eq} \cdot s^3} \quad (A3.3)$$

A.4 Mechanical properties of considered connections

Table A.1 contains the data used to define the top connection hysteretic behaviour. The application of the proposed analytical formulation leads to the values summarized in **Table A.2**. The lateral force–displacement relationship of the bottom connections is directly evaluated considering the bolt flexibility for BC1 (ϕ_b 24mm; $L_b = 50$ mm; $f_u = 640$ MPa) and the flexural stiffness of the tapered steel plate for BC2, modelled as a triangular element with edges 100mm x 130mm and thickness 20mm, $f_u = 350$ MPa.

The top and bottom connections are simulated in the FE models by one or more nonlinear springs acting in parallel: **Table A.3** summarizes the considered hysteresis models. **Table A.4** shows the combination of the springs in order to obtain the global behaviour of the considered connections.

In PCS A and PCS B the top connections fails before sliding of the bottom connection, therefore only a spring is provided in BC1. TC1 failure is associated to anchor channel lip. The failure load (11.77 kN) derived from the analytical procedure is lower than recorder during the tests, therefore on the conservative side. Besides this, the numerical investigation was carried out considering the failure load recorded in the tests.

In PCS C/D the top connection develops two plastic hinges at the bolt ends, causing the bolt rotation until contact between the nut and the panel. At this stage, the connection gains stiffness and the lateral load increases until failure of the weakest component: the bolt in shear (27.6 kN according to

Eurocode 3). A more accurate description of the connection and bolt behaviour after the contact to the panel could be obtained from refined tridimensional finite element models.

The friction load associated to sliding of TC1, TC2 and BC2 is taken directly from the test results.

A.5 Equivalent stiffness

In this section, the equivalent stiffness of the case-study column is evaluated.

Based on the data of **Table A.5** the flexural stiffness at yield is:

$$EI_y = \frac{M_y}{\phi_y} = 9.96 \times 10^{13} \text{ Nmm}^2 \quad (\text{A3.3})$$

The stiffness reduction factor is the ratio between the flexural stiffness at yield and the gross stiffness:

$$\frac{EI_y}{EI_g} = \frac{9.96 \times 10^{13} \text{ Nmm}^2}{3.564 \times 10^{14} \text{ Nmm}^2} = 0.28 \quad (\text{A3.3})$$

References

ABAQUS user's manual version 6.11 (2011) Dassault Systèmes Simulia Corp.

Ambraseys N., Smit P, Douglas J et al. (2004) Internet-site for European strong-motion data.
Bollettino di Geofisica Teorica ed Applicata, 45(3), 113–129

Arnold C (1989) Cladding design: architectural trends and their influence on seismic design.
Proceedings: Architectural Precast Concrete Cladding – It's Contribution to Lateral Resistance of Buildings. PCI, November 8-9, Chicago

Baker JW, Cornell CA. (2006) Spectral shape, epsilon and record selection. Earthquake Engineering and Structural Dynamics, 35(9):1077–1095.

Belleri A, Riva P. (2012) Seismic performance and retrofit of precast concrete grouted sleeve connections. PCI Journal, 57(1):97-109

- Belleri A, Torquati M, Riva P (2014a) Seismic performance of ductile connections between precast beams and roof elements. *Magazine of Concrete Research*, 66(11):553-562, doi:10.1680/macr.13.00092
- Belleri A, Brunesi E, Nascimbene R, Pagani M, Riva P (2014b) Seismic Performance of Precast Industrial Facilities Following Major Earthquakes in the Italian Territory. *J. Perform. Constr. Facil.*, doi:10.1061/(ASCE)CF.1943-5509.0000617
- Belleri A, Torquati M, Riva P, Nascimbene R (2015) Vulnerability assessment and retrofit solutions of precast industrial structures. *Earthquake and Structures*, 8(3):801-820 doi:10.12989/eas.2015.8.3.801
- Biondini F, Dal Lago B, Toniolo G (2013) Role of wall panel connections on the seismic performance of precast structures. *Bulletin of Earthquake Engineering*, 11(4):1061-1081
- Brunesi E, Nascimbene R, Bolognini D, Bellotti D (2015) Experimental investigation of the cyclic response of reinforced precast concrete framed structures. *PCI Journal*, 15(2):57-79
- BSI (2005) BS EN 1998–1: 2004. Eurocode 8: Design of structures for earthquake resistance. Part 1: General rules, seismic actions and rules for buildings. BSI, London, UK
- Colombo A, Negro P, Toniolo G (2014) The influence of claddings on the seismic response of precast structures: the safecladding project. *Proceedings of 2nd ECEES: 24-29 August 2014, Istanbul, Turkey*
- Ferrara L, Felicetti R, Toniolo G, Zenti C (2011) Friction dissipative devices for cladding panels in precast buildings. *European Journal of Env. and Civil Engineering*, 15(9):1319-1338
- Fischinger M, Zoubek B, Isakovic T (2014) Seismic response of precast industrial buildings. *Perspectives on European Earthquake Engineering and Seismology: Vol. 1*. Ansal A (editor), Springer, Berlin, pp 131-177
- Haber ZB, Saiidi MS, Sanders DH (2014) Seismic Performance of Precast Columns with Mechanically Spliced Column-Footing Connections. *Aci Structural Journal*, 111(3):639-650

- Isakovic T, Zoubek B, Lopatic J, Fischinger M (2014) Experimental research of typical cladding panel connections in industrial buildings. Proceedings of 2nd ECEES: 24-29 August 2014, Istanbul, Turkey
- Kramar M, Isakovic T, Fischinger M (2010) Seismic collapse risk of precast industrial buildings with strong connections. *Earthquake Engineering & Structural Dynamics*, 39(8):847-868
- Liberatore L, Sorrentino L, Liberatore D, Decanini LD (2013) Failure of industrial structures induced by the Emilia (Italy) 2012 earthquakes. *Engineering Failure Analysis*, 34:629-647
- Magliulo G, Ercolino M, Manfredi G (2014a) Influence of cladding panels on the first period of one-story precast buildings, *Bulletin of Earthquake Engineering*, doi:10.1007/s10518-014-9657-2
- Magliulo G, Ercolino M, Petrone C, Coppola O, Manfredi G (2014b) The Emilia Earthquake: Seismic Performance of Precast Reinforced Concrete Buildings. *Earthquake Spectra*, 30(2):891-912
- Metelli G, Beschi C, Riva P (2011) Cyclic behaviour of a column to foundation joint for concrete precast structures, *European Journal of Environmental and Civil Engineering*, 15(9):1297-1318
- MidasGEN 2012 (v3.1), MIDAS Information Technologies Co. Ltd.
- National Institute of Standards and Technology, NIST GCR 95-681 (1995) Literature Review on Seismic Performance of Building Cladding Systems
- National Institute of Standards and Technology, NIST GCR 98-758 (1998) Ductile Cladding Connection Systems for Seismic Design
- Osanai Y, Watanabe F, Okamoto S (1996) Stress transfer mechanism of socket base connections with precast concrete columns. *Aci Structural Journal*, 93(3):266-276
- Pinelli JP, Craig JI, Goodno BJ (1995) Energy-Based Seismic Design Of Ductile Cladding Systems. *Journal of Structural Engineering-ASCE*, 121(3):567-578
- Pinelli JP, Moor C, Craig JI, Goodno BJ (1996) Testing of energy dissipating cladding connections. *Earthquake Engineering & Structural Dynamics*, 25(2):129-147

- Toniolo G, Colombo A (2012) Precast concrete structures: the lessons learned from the L'Aquila earthquake. *Structural Concrete*, 13:73-83
- Vamvatsikos D, Cornell CA (2002) Incremental dynamic analysis. *Earthquake Engineering and Structural Dynamics*, 31(3):491–514
- Venmarcke EH, Gasparini DA (1976) Simulated Earthquake Motions Compatible with Prescribed Response Spectra – SIMQKE-1. M.I.T. Department of Civil Engineering Research Report R76-4
- Wang ML (1987) Cladding Performance on a Full Scale Test Frame. *Earthquake Spectra*, 3(1):119-173

TABLES

Table 1 Period and mass participation factor comparison

	T ₁ (s)	m ₁ (%)	T ₂ (s)	m ₂ (%)	T ₃ (s)	m ₃ (%)
Point mass	1.57	83.2	0.14	5.0	0.11	4.0
PCS ideal	1.54	80.0	0.12	8.9	0.04	2.2
PCS A/B	0.89	81.1	0.12	8.3	0.06	1.9
PCS C/D	0.74	83.0	0.11	8.2	0.07	1.9

Table 2 Response spectrum analyses results for SLS and DBE.

		Point mass	PCS ideal	PCS A/B	PCS C/D
SLS	Column base shear (kN)	63.4	58.2	72.8	80.5
	Inter-storey drift (%)	0.82	0.79	0.46	0.39
	PCS rotation (rad x 100)	1.19	1.16	0.62	0.49
DBE q=2	Column base shear (kN)	79.5	73.1	91.2	100.8
	Inter-storey drift (%)	1.01	0.99	0.57	0.49
	PCS rotation (rad x 100)	1.48	1.45	0.77	0.62

Table 3 Time history analyses results for SLS and DBE.

		Point mass	PCS ideal	PCS A	PCS B	PCS C/D
SLS	Column base shear (kN)	84.1	66.1	55.5	70.3	55.8
	Inter-storey drift (%)	0.97	0.87	0.37	0.74	0.49
	PCS rotation (rad x 100)	1.35	1.18	0.50	1.00	0.69
DBE	Column base shear (kN)	116.8	120.2	113.3	121.2	120.3
	Inter-storey drift (%)	1.49	1.43	1.56	1.51	1.51
	PCS rotation (rad x 100)	2.01	1.94	2.14	2.01	2.04

TABLES IN APPENDIX A

Table A.1 Properties of top connections

Data		TC1	TC2
f_u	(MPa)	250	350
s	(mm)	2.5	2.5
t	(mm)	8	8
i	(mm)	20	20
h	(mm)	22	22
d	(mm)	35.75	35.75
e	(mm)	29.5	29.5
EI_{sl}	(kN mm ²)	42600	42600
L_{sl}	(mm)	120	120
ϕ_b	(mm)	16	14
L_b	(mm)	80	55

Table A.2 Application of the analytical formulations – Top connections

TC1			TC2		
Failure: anchor channel lip			Failure: bolt in shear after contact to panel side		
$k_{\theta S1}$	(kN/mm)	5973	$k_{\theta S1}$	(kN/mm)	5973
F_{max} (Eq.1)	(kN)	8.20	M_{yb}	(kN/mm)	228.67
b_{eq} (Eq.2)	(mm)	35	$\theta_{S1, I^{yielding}}$ (Eq.6)	(rad)	0.01517
Δ_{eq} (Eq.3)	(mm)	0.06	$\theta_{S2, I^{yielding}}$ (Eq.7)	(rad)	0.00559
Δ_{tot} (Eq.4)	(mm)	0.21	$\theta_{S1, II^{yielding}}$ (Eq.6)	(rad)	0.02311
$k_{\theta S2}$	(kN/mm)	40914	$\theta_{S2, II^{yielding}}$ (Eq.7)	(rad)	0.03269
k_{TC} (Eq.5)	(kN/mm)	3.78	k_{TC} (Eq.5)	(kN/mm)	7.50
$k_{TC-post yield}$ (Eq.5)	(kN/mm)	0.76	$k_{TC-post yield}$ (Eq.5)	(kN/mm)	1.55

Table A.3 Basic nonlinear springs adopted in the numerical simulations

<i>A – Normal bilinear</i>	<i>B – Clough</i>	<i>C – Slip trilinear</i>
----------------------------	-------------------	---------------------------

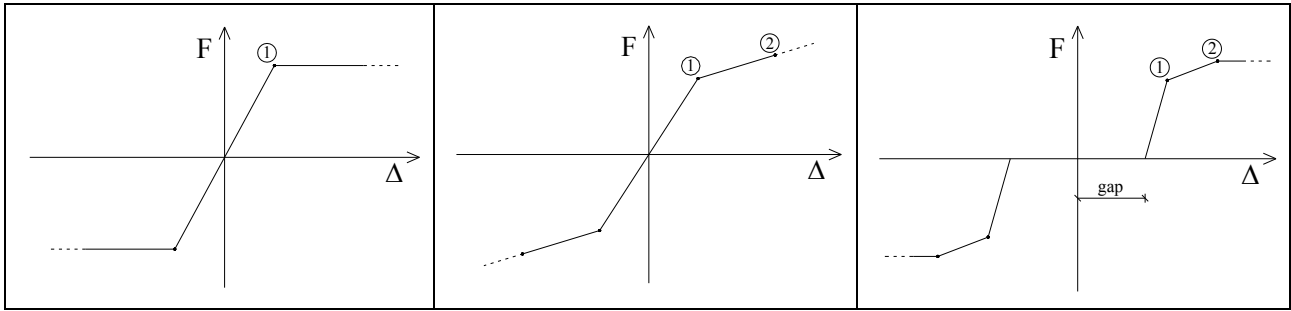


Table A.4 Hysteresis models used for each connection and definition of the main points

	Connection	Hysteresis type	Main points
PCS A	TC1	B	$F_1 = 4.2\text{kN}; \Delta_1 = 1.1\text{mm}$ $F_2 = 11.8\text{kN}; \Delta_2 = 11.2\text{mm}$ $(F_2 = 16.4\text{kN}; \Delta_2 = 25.9\text{mm}$ - failure load from test)
	BC1	A	$F_1 = 23.5\text{kN}; \Delta_1 = 8.3\text{mm}$
PCS B	TC1	A (Friction)	$F_1 = 2\text{kN}; \Delta_1 = 0.5\text{mm}$
		C (Yielding)	$F_1 = 2.2\text{kN}; \Delta_1 = 20.6\text{mm}$ $F_2 = 9.8\text{kN}; \Delta_2 = 33.2\text{mm}$ $(F_2 = 16.4\text{kN}; \Delta_2 = 49.4\text{mm}$ - failure load from test) gap = 20mm
	BC1	A	$F_1 = 23.5\text{kN}; \Delta_1 = 8.3\text{mm}$
PCS C/D	TC2	A (Friction)	$F_1 = 4.5\text{kN}; \Delta_1 = 0.6\text{mm}$
		C (Yielding)	$F_1 = 1.3\text{kN}; \Delta_1 = 35.2\text{mm}$ $F_2 = 3.8\text{kN}; \Delta_2 = 36.8\text{mm}$ gap = 35mm
		C (Contact)	$F_1 = 12\text{kN}; \Delta_1 = 46.6\text{mm}$ $F_2 = 25\text{kN}; \Delta_2 = 67.7\text{mm}$ gap = 45mm
	BC2	A (Friction)	$F_1 = 17\text{kN}; \Delta_1 = 0.46\text{mm}$
		C (Yielding)	$F_1 = 29.2\text{kN}; \Delta_1 = 25.8\text{mm}$ $F_2 = 29.2\text{kN}; \Delta_2 = 40\text{mm}$ gap = 25mm

Table A.5 Properties of the column

Axial load	N	(kN)	670
Modulus of elasticity	E_c	(MPa)	33000
Ultimate moment	M_u	(kNm)	650
Yield moment	M_y	(kNm)	495
Curvature at yield	ϕ_y	(rad/mm)	4.97×10^{-6}

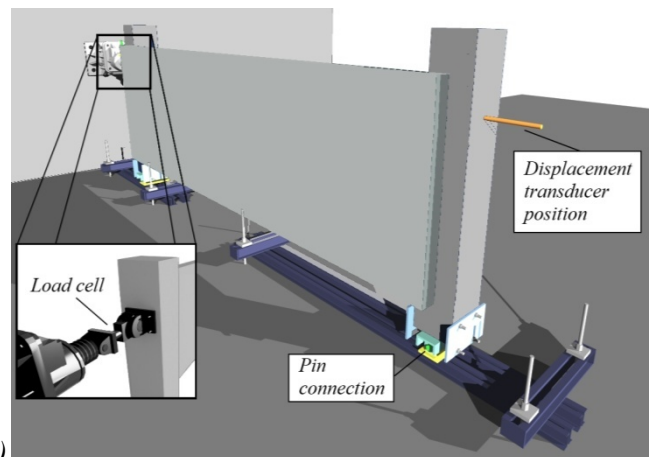
FIGURES



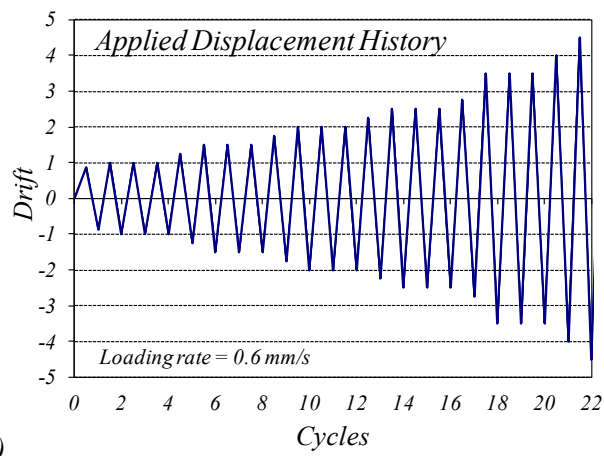
Fig. 1 Horizontal cladding failure after a seismic event



a)



b)



c)

Fig. 2 Cladding panel subassembly test setup

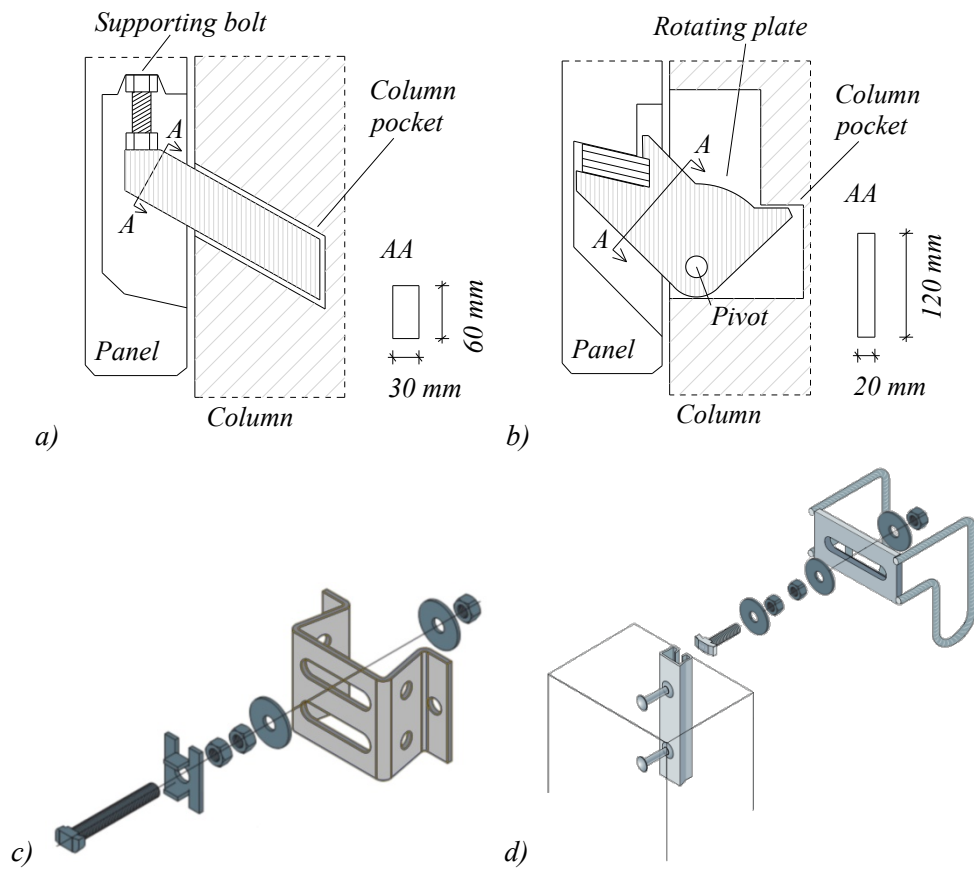


Fig. 3 Considered top and bottom connections.
 (a) Bottom connection 1 (BC1); (b) Bottom connection 2 (BC2);
 (c) Top connection 1 (TC1); (d) Top connection 2 (TC2)

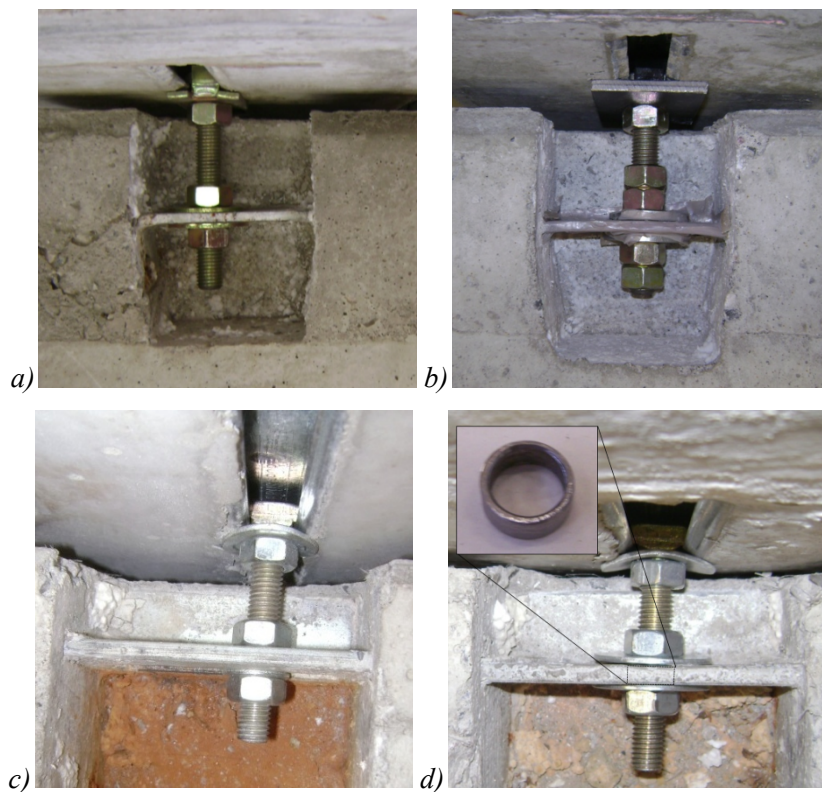


Fig. 4 Panel Column Subassembly (PCS) top connection details.
 (a) PCS A; (b) PCS B; (c) PCS C; (d) PCS D

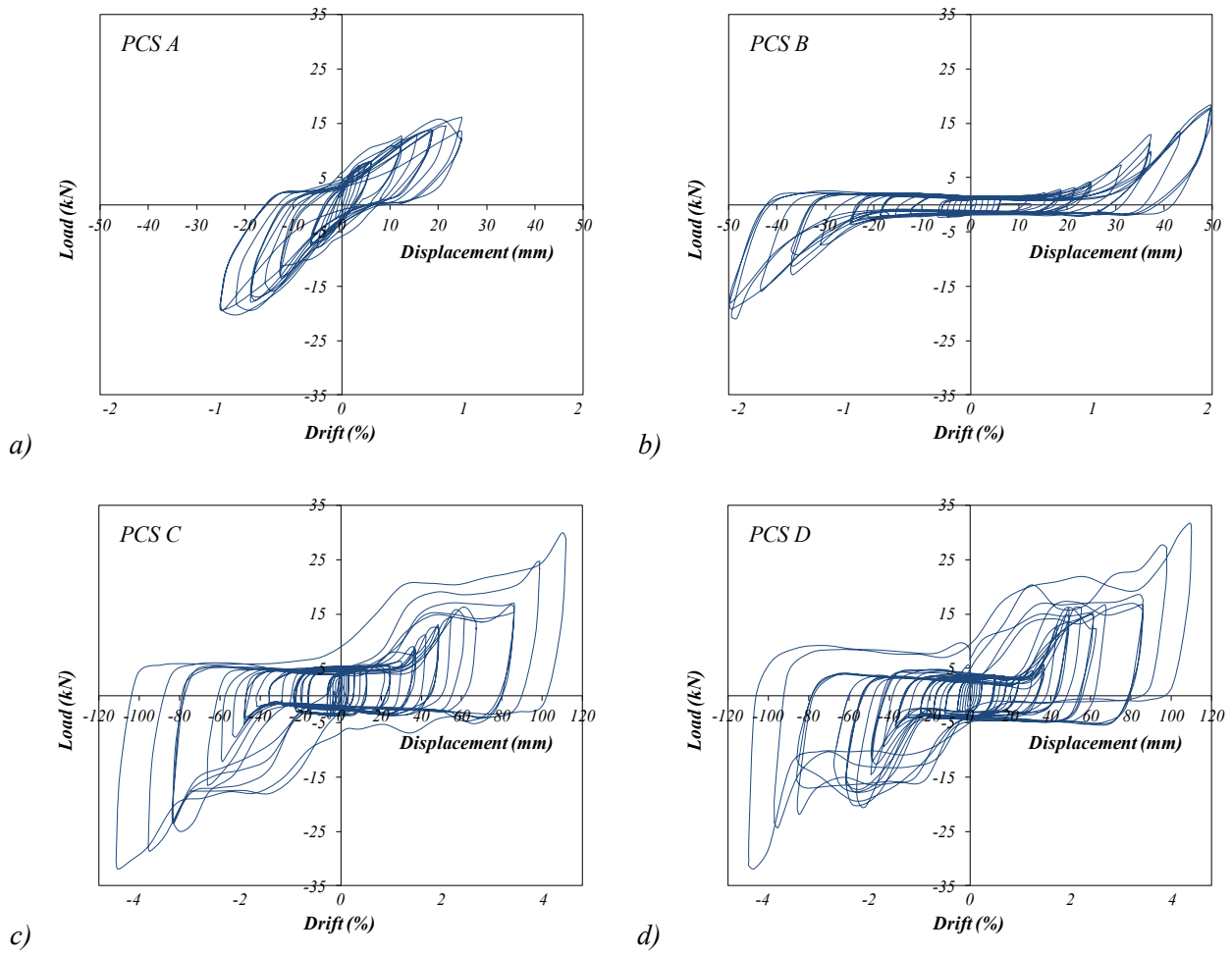


Fig. 5 Panel Column Subassembly (PCS) lateral load-displacement graphs

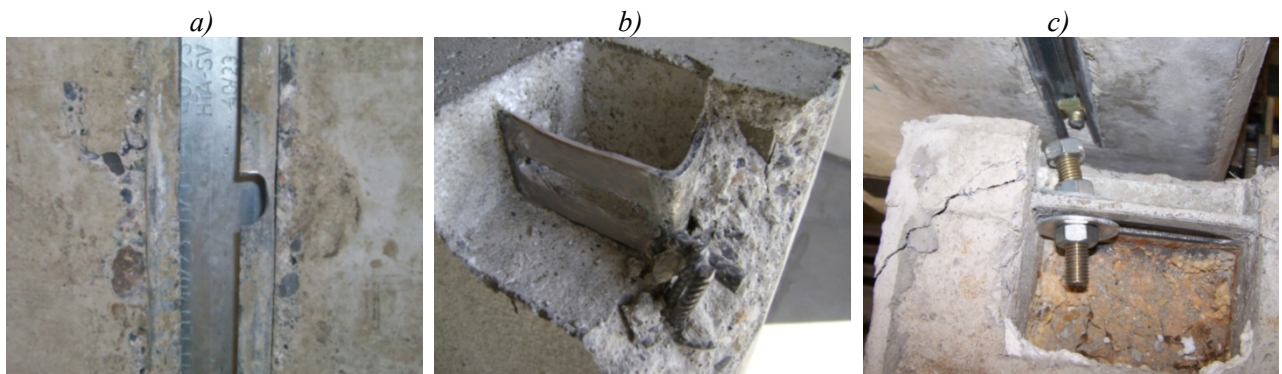


Fig. 6 Top connection failure mechanisms: (a) PCS A, (b) PCS B, (c) PCS D

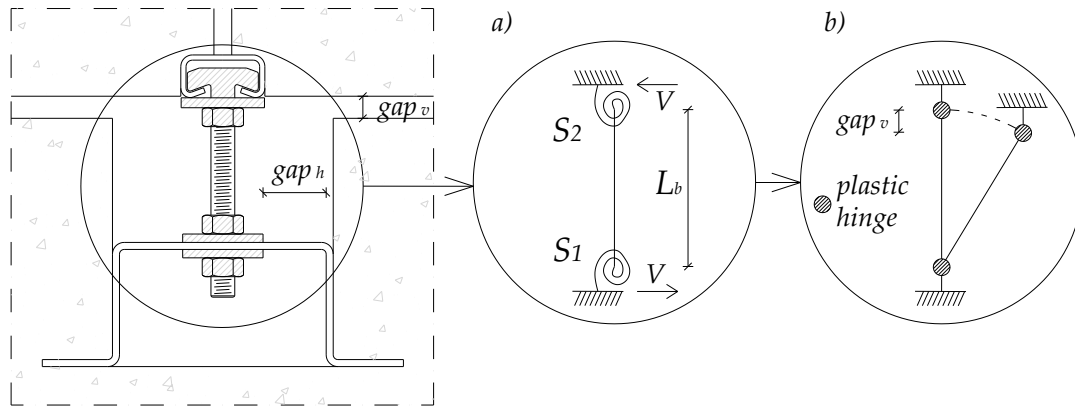


Fig. 7 Static scheme of top connection

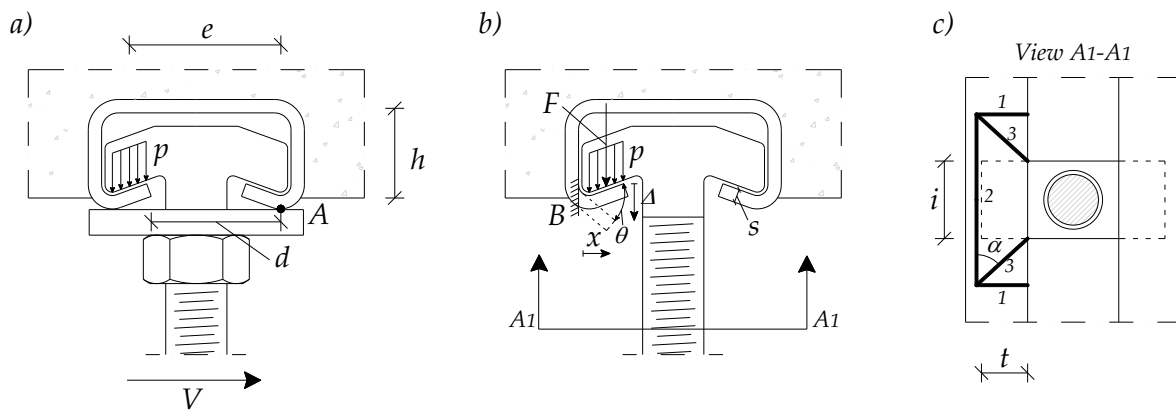


Fig. 8 Anchor channel behaviour

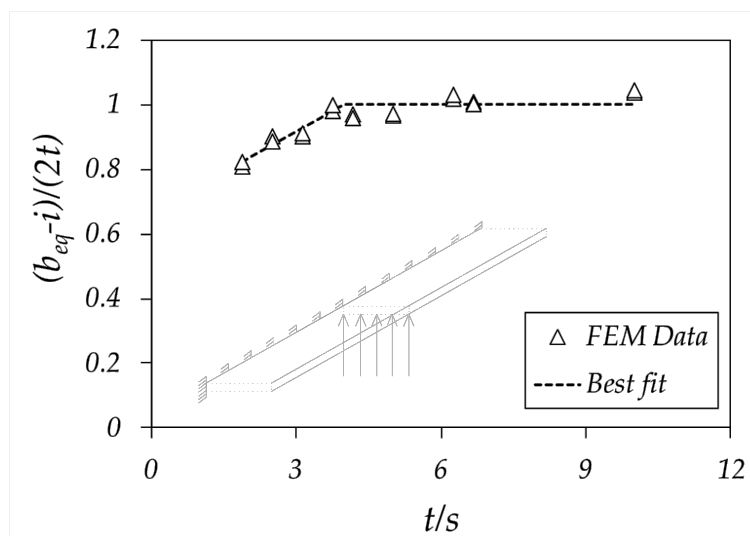


Fig. 9 Beam equivalent depth evaluation graph

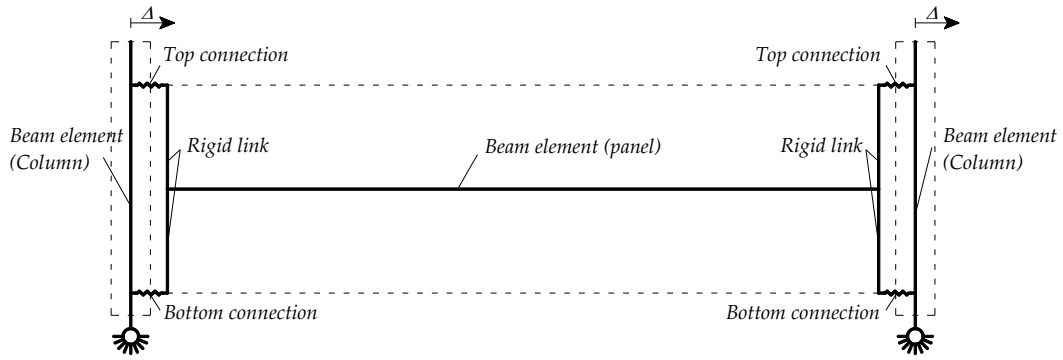


Fig. 10 Scheme of the considered numerical model resembling the test setup

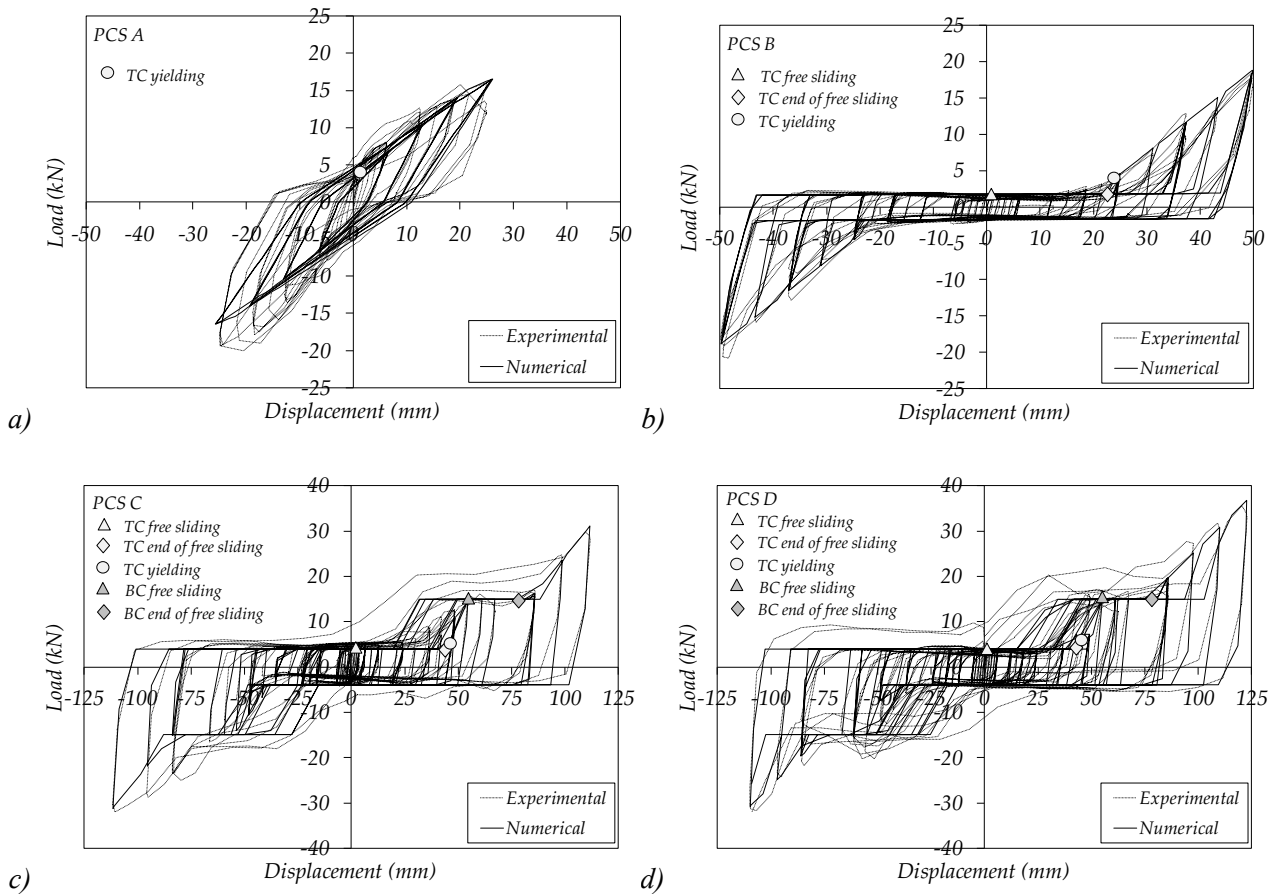
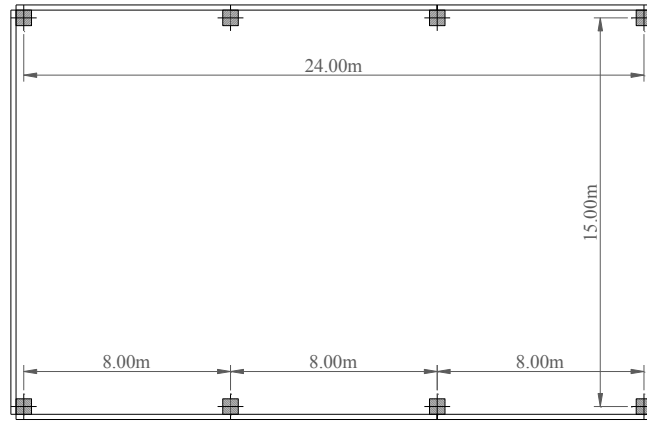


Fig. 11 Experimental and analytical results comparison

Plan view



Side view

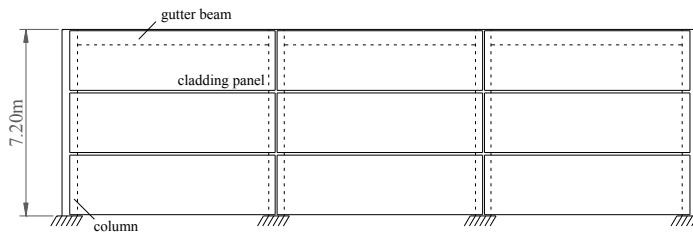


Fig. 12 Considered case study

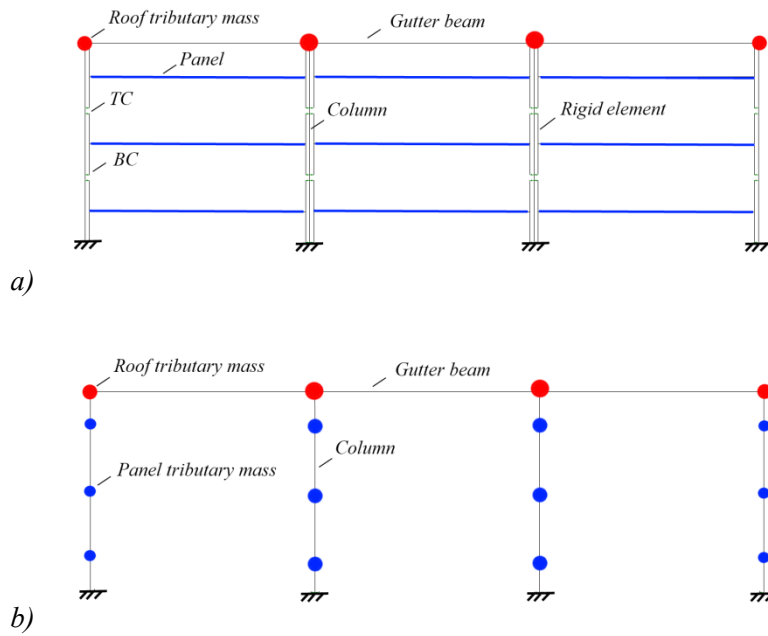


Fig. 13 Considered finite element models

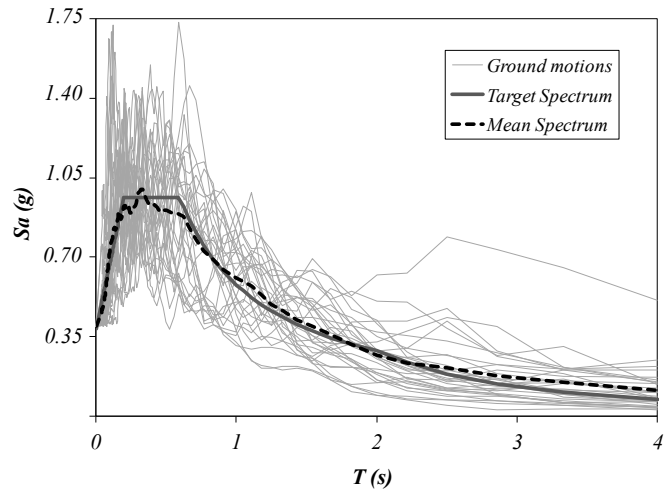
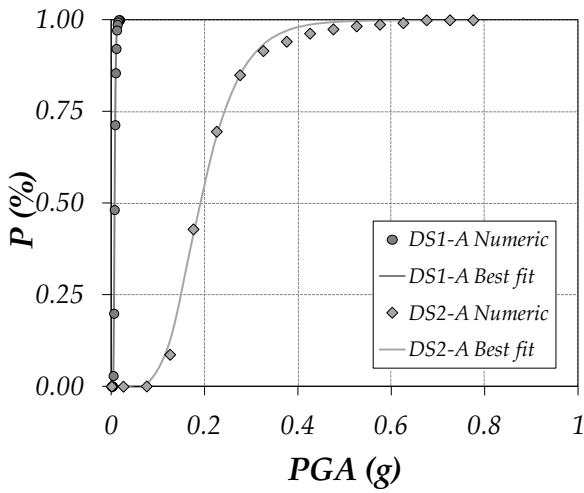
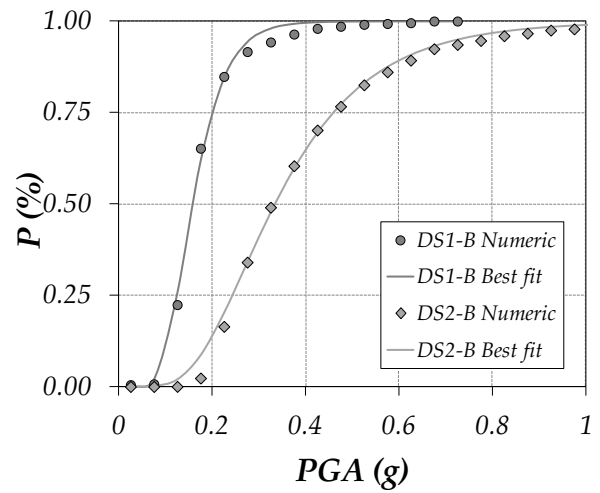


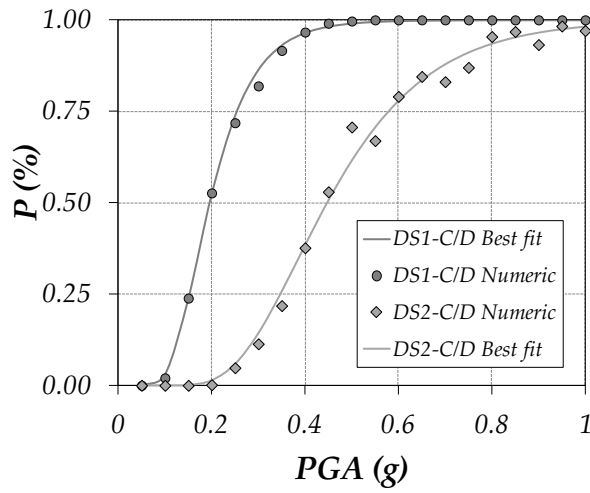
Fig. 14 Pseudo acceleration spectra ($\xi = 0.05$)



a)



b)



c)

Fig. 15 Fragility curves for (a) PCS A (b) PCS B and (c) PCS C/D connections

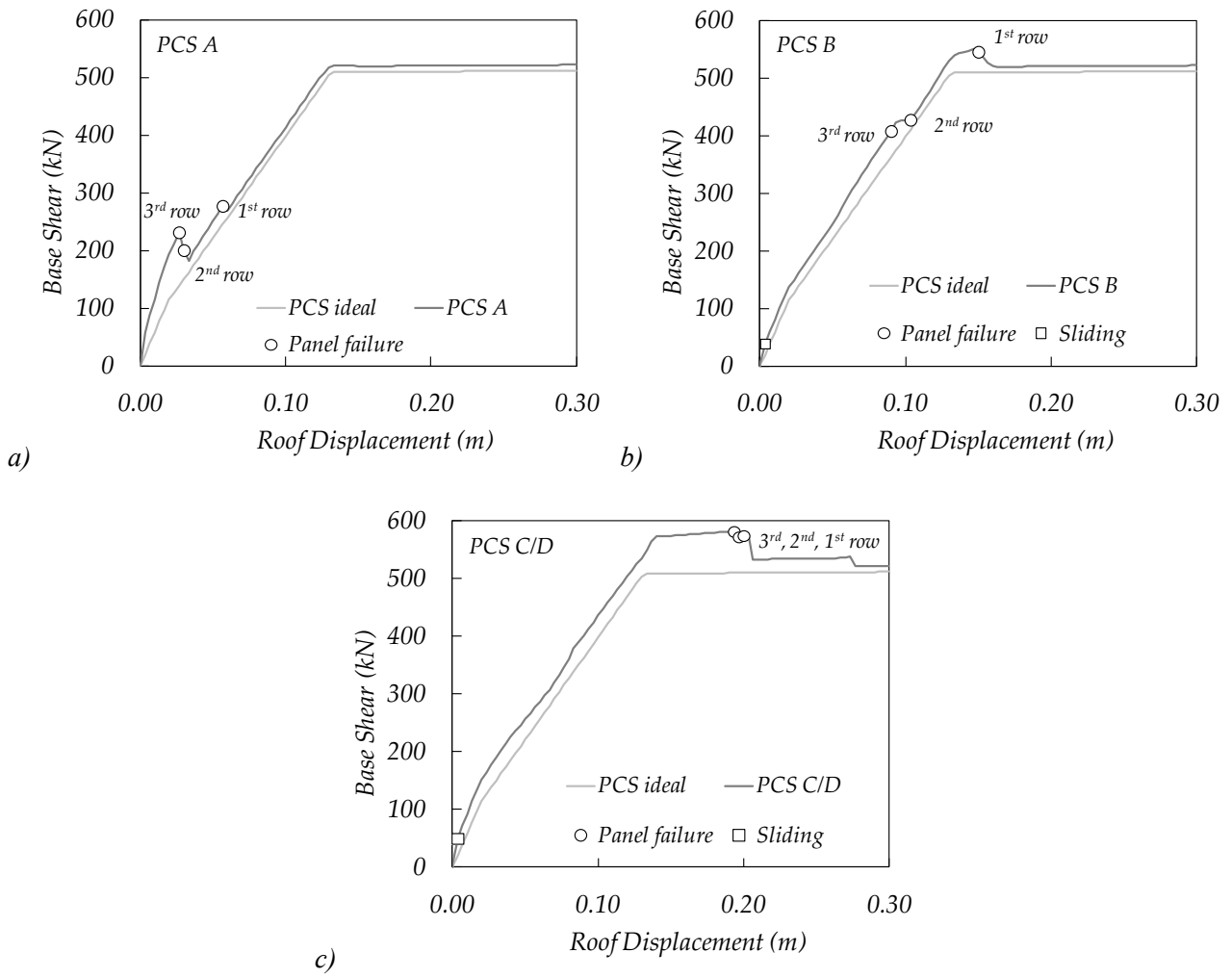


Fig. 16 Pushover results for (a) PCS A (b) PCS B and (c) PCS C and PCS D connections

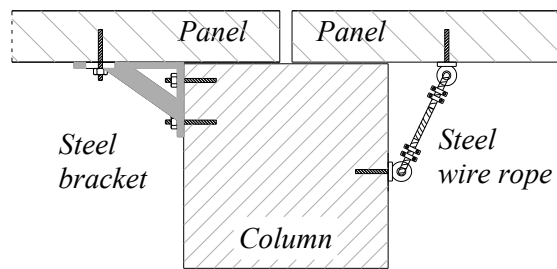


Fig. 17 Possible out-of-plane back-up solutions